

## ESTIMATION OF THE SHEAR-WAVE VELOCITY OF SHALE-OIL RESERVOIRS: A CASE STUDY OF THE CHANG 7 MEMBER IN THE ORDOS BASIN

ZHIJIAN FANG<sup>1</sup>, JING BA<sup>1\*</sup>, JOSÉ M. CARCIONE<sup>1,2</sup>, WENSHAN LIU<sup>1</sup> and CHANGSHENG WANG<sup>3</sup>

<sup>1</sup> School of Earth Sciences and Engineering, Hohai University, Nanjing 211100, P.R. China. [jingba@188.com](mailto:jingba@188.com)

<sup>2</sup> National Institute of Oceanography and Applied Geophysics (OGS), Trieste, Italy.

<sup>3</sup> Exploration and Development Research Institute of PetroChina Changqing Oilfield Company, Shanxi, Xi'an 710018, P.R. China.

(Received June 16, 2021; accepted November 11, 2021)

### ABSTRACT

Fang, Z.J., Ba, J., Carcione, J.M., Liu, W.S. and Wang, C.S., 2022. Estimation of the shear-wave velocity of shale-oil reservoirs: a case study of the Chang 7 member in the Ordos basin. *Journal of Seismic Exploration*, 31: 81-104.

The absence of shear-wave (S-wave) log data restricts the geophysical characterization and fluid identification of Chang 7 shale-oil reservoirs in Ordos Basin, and we have to make use of suitable rock-physics theories to overcome this problem. We reformulate the Xu-White model by combining the critical-porosity and Maxwell-BISQ models to predict the S-wave velocity, where the BISQ model includes a non-Newtonian (Maxwell) fluid. The approach takes into account rock composition, pore structure, fluid properties and saturation. Three wells with S-wave log data are considered to verify the feasibility of the method. The results show that the proposed reformulated approach is suitable for S-wave velocity estimation.

KEY WORDS: shale oil, S-wave velocity prediction, Maxwell fluid, Xu-White model, critical porosity model, BISQ model.

### INTRODUCTION

The shear wave (S-wave) velocity plays an important role, as the compressional wave (P-wave) velocity and rock density, for AVA and AVO analysis of seismic data (Downton, 2005), pre-stack seismic inversion, reservoir property prediction and fluid identification (Smith and Gidlow, 2000; Pang et al., 2017). Specifically, when conducting seismic inversion based on log data, S-wave velocity is essential (e.g., Vernik et al., 2017).

However, due to technical and economical issues, S-wave logging is relatively infrequent (Tan et al., 2015). Empirical equations and rock-physics models can then be of great help in this sense (Li et al., 2017; Ba et al., 2017; Zhang et al., 2019; Zhang et al., 2021).

Based on P-wave log data, porosity, rock mineral composition, shale content and density, empirical equations for several rocks (dolomite, limestone, sandstone and shale) can be established (Pickett et al., 1963; Castagna et al., 1985; Li, 1992). Han et al. (1986) measured 75 sandstone samples as a function of pressure and obtained a linear regression equation between the velocities. Krief et al. (1990), based experiments and theory, found a relationship between the squares of the P- and S-wave velocities. However, empirical relations have mostly a local validity. A useful approach is to employ neural networks, which use well-log data as training, and then predict reservoir properties (e.g., Qadrouh et al., 2019). Gholami et al. (2014) analyzed seismic attributes based on the independent variable analysis to predict S-wave velocity, and Parvizi et al. (2015) used genetic algorithms and artificial neural network this prediction.

Xu and White (1995,1996) proposed a theoretical model for sand and mudstone formations, by combining the differential effective medium theory, Kuster-Toksöz model (1974) and Gassmann equation (1951). In their model, the pore aspect ratio is assumed to be constant (generally that mudstone is in the range 0.03-0.04 and that of sandstone in the range 0.1-0.12). However other studies have shown that the pore aspect ratio is not constant, and it is affected by temperature, depth, pressure, etc., and varies over a wide range (Nur and Simmons, 1969; Brown and Korringa, 1975). Yan et al. (2007) proposed an empirical equation for estimating the aspect ratio of sandstone pores as a function of depth.

In addition to the classic empirical and theoretical models, there are methods that combine theoretical and empirical models. Nur et al. (1992) assumed that the dry-rock modulus is linearly related to rock porosity, and proposed a critical porosity model. Biot (1956a, 1956b, 1962) proposed dynamic equations for wave propagation in fluid-saturated porous media and showed the existence of a slow P-wave, while Mavko and Nur (1975) introduced the squirt-flow mechanism based on a microscopic pore description, describing high-frequency velocity dispersion and attenuation. Dvorkin and Nur (1993) assumed that the pores are saturated with single fluid and presented the BISQ model. Dvorkin et al. (1994) further extended this model to partially saturated conditions by modifying the characteristic squirt length. Moreover, it is important to model the non-Newtonian (Maxwell) behavior of the fluids (Tsiklarui, 2002; Cui et al., 2003, 2010).

Shale oil, an unconventional resource, is a relatively new field in petroleum production (e.g., Zou et al., 2013; EIA, 2013). As marine shale oil in the United States (Zhang et al., 2015), China's continental shale oil also has contained huge prospects for future exploration and development. Recently, China has discovered shale-oil resources in the Ordos Basin

(Zhou et al., 2018). The Chang 7 Member of this basin has high-quality reservoirs. We reformulate the Xu-White model by combining the critical-porosity and Maxwell-BISQ models to predict the S-wave velocity of these reservoirs. The methodology is applied to three wells from the work area.

## TARGET FORMATION AND SHALE OIL RESERVOIR CHARACTERISTICS

### Overview of the working area

The Ordos Basin is a large stable polycyclic craton basin located in China with a gentle westward dipping monocline. It can be divided into six tectonic units, of which the Tianhuan Syncline and the Northern Shaanxi Slope are the main units (Fig. 1), and also the main hydrocarbon distribution areas. The Northern Shaanxi Slope, with the largest area, is the main distribution unit of Paleozoic natural gas and Mesozoic oil. Since the Late Triassic, the Ordos Basin has gradually been transformed into an inland lacustrine sedimentary environment, where the Yanchang Formation located in the Upper Triassic presents a set of fluvial-deltaic-lacustrine clastic rocks. The Yanchang Formation is divided into 10 oil formations, including the Chang 7 Member. The study area is located at the interchange of provenance in the southwest and northeast of the basin. The oil in the tight sandstone and shale within the source rocks, without long-distance migration and accumulation, is a typical shale oil, of high-quality in Changqing Oilfield. The Chang 7 formation became the main exploration layer in recent years.

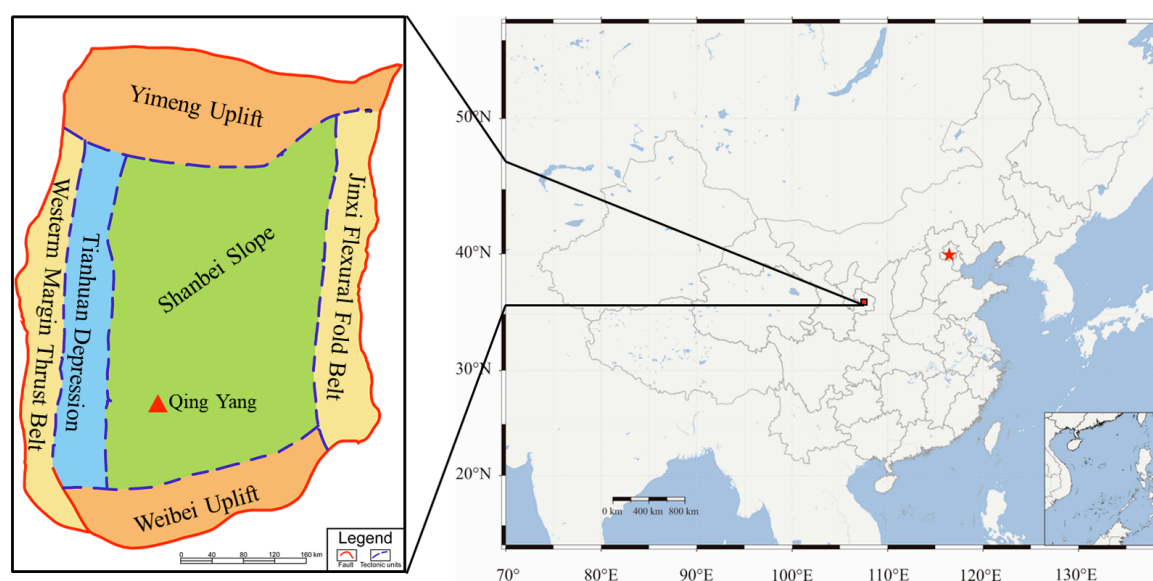


Fig. 1. Location of the Qingyang area in the Ordos Basin.

## Lithologic characteristics of the target strata

There are three types of shale-oil rocks in the Chang 7 Member of the Yanchang Formation. The first type is multi-stage superimposed sandstone. The reservoirs are mainly fine sandstones with medium thickness. Type 2 is shale with thin-layer sandstones (the reservoir). The content of quartz and feldspar in the rocks is generally more than 50%, and the thickness of a single sand body is 2 ~ 5 m. Type 3 is pure shale, and the reservoir is mainly organic rich dark mudstone and black shale, with quartz and feldspar content up to 50%, plus carbonate and pyrite. The content of brittle components can reach more than 70%, and the thickness of a single sand body is less than 2 m.

Type 1 and 2 shale oil are mainly developed in the members of Chang 7<sub>1</sub>~ Chang 7<sub>2</sub>, while Type 3 is more common in Chang 7<sub>3</sub>. We mainly consider the Chang 7<sub>1</sub>~ Chang 7<sub>2</sub> Members. Fig. 2 shows cores and thin section observed in the laboratory. The thin section shows that the composition mainly ranges from fine sand to very fine sand, and the interstitials are mainly carbonate minerals with a small amount of clay minerals, of which calcite is dominant and dolomite follows.

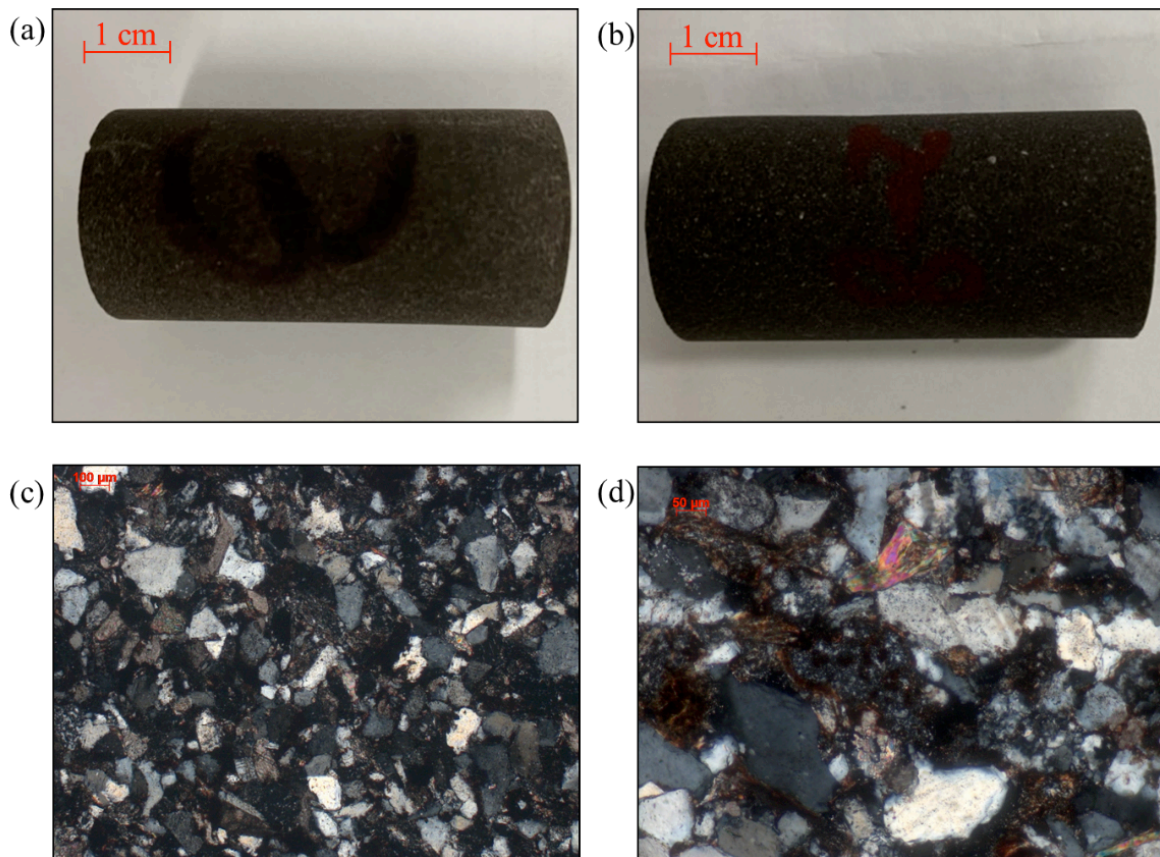


Fig. 2. Cores and thin sections of the Chang 7<sub>1</sub>~ Chang 7<sub>2</sub> Member, Ordos Basin.  
 (a) Chang 7<sub>1</sub> core; (b) Chang 7<sub>2</sub> core; (c) thin section of Chang 7<sub>1</sub>; (d) thin section of

Chang 7<sub>2</sub>.

## Log-data analysis

The physical properties of Chang 7 Member reservoirs show that the porosity is in the range 4 ~ 12%, and the permeability is in the range 0.01 ~ 0.50 mD (Fig. 3), which indicate tight reservoirs. Figs. 4 and 5 show the wave velocities as a function of porosity for different water saturations and shale content, respectively. Water saturation (shale content) are be divided into two ranges: 0 ~ 50% and 50 ~ 100% are the low and high saturation (shale content) areas, respectively. As indicated by the red line, delimiting different areas, both the P- and S-wave velocities decrease with increasing porosity. In addition, the velocities decrease for increasing shale content (e.g., Carcione et al., 2000).

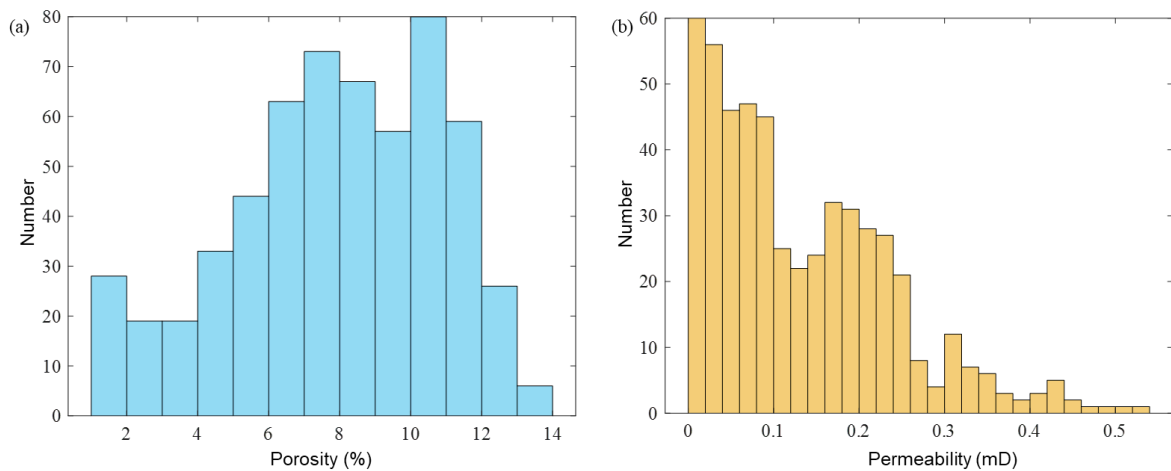


Fig. 3. Statistical distribution of porosity (a) and permeability (b) of the cores.

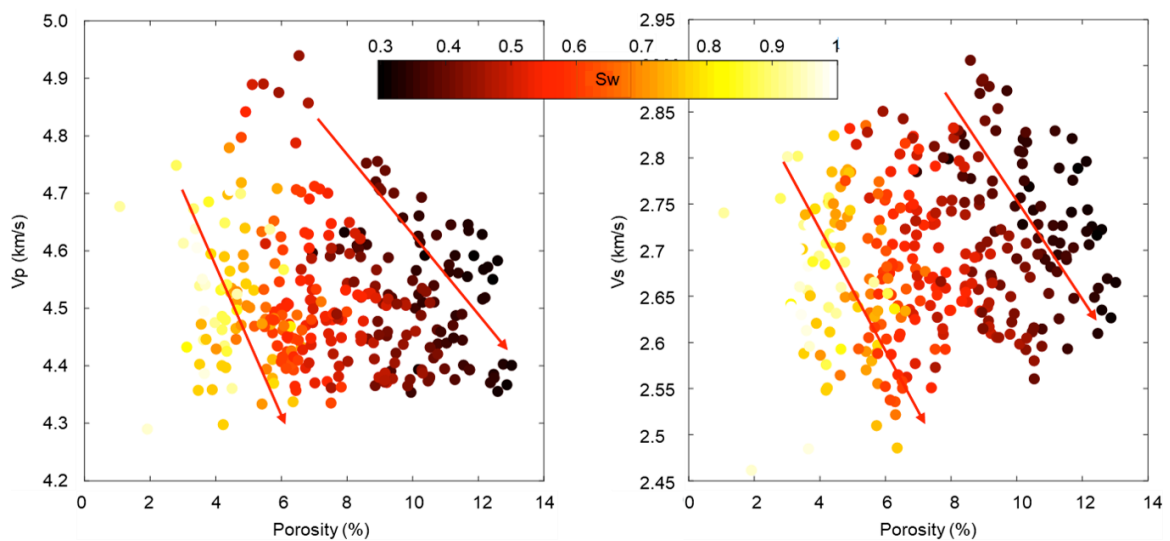


Fig. 4. P- (a) and S-wave (b) velocity as a function of porosity for different water saturations.

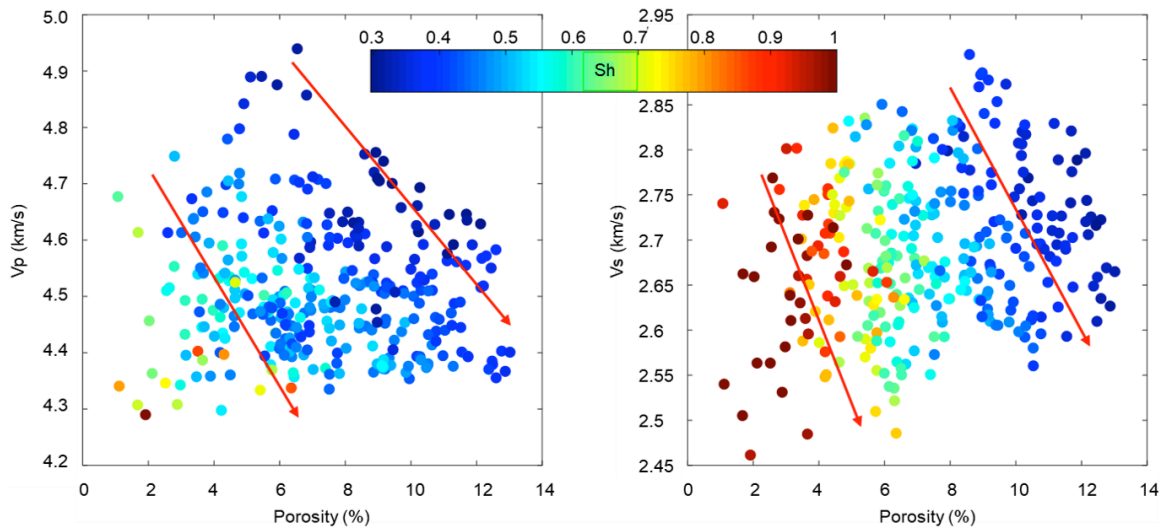


Fig. 5. P- (a) and S-wave (b) velocity as a function of porosity for different. shale content.

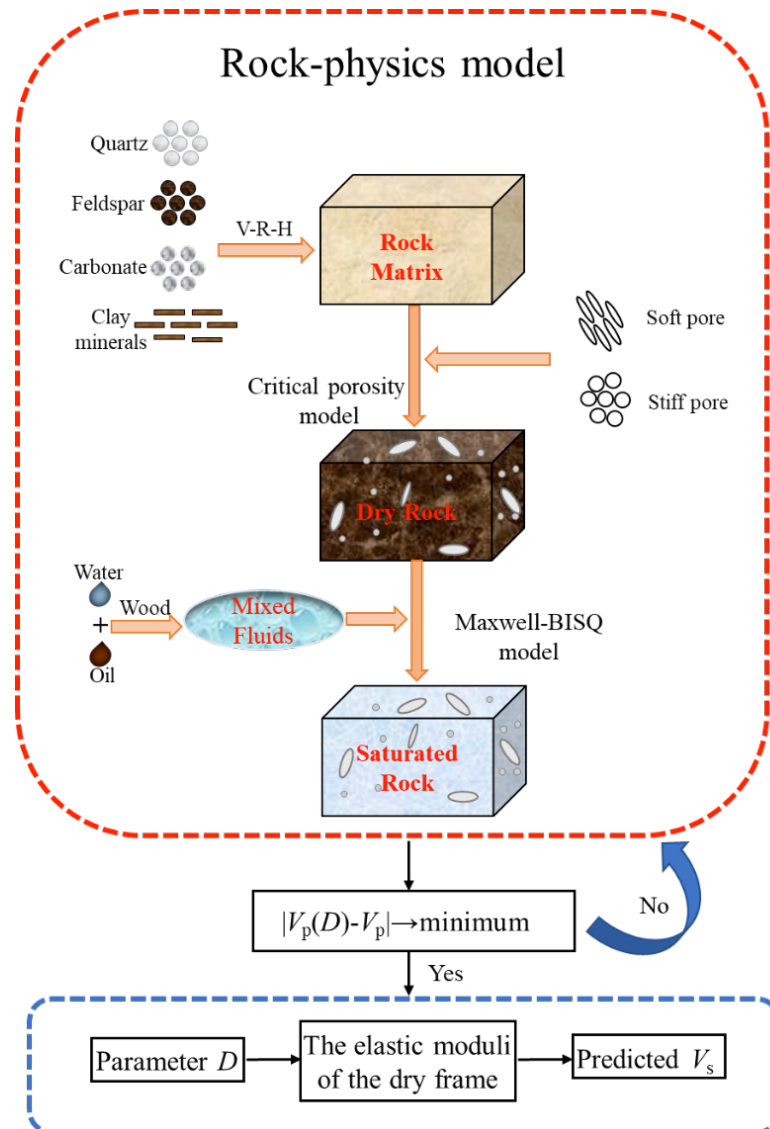


Fig. 6. Rock-physics modeling flow chart.

## THEORY AND METHODS

The Chang 7 Member can be roughly divided into two lithological sections, of which the Chang 7<sub>1</sub>-Chang 7<sub>2</sub> Members are mainly tight sandstone and siltstone and the Chang 7<sub>3</sub> Member is mainly pure shale. We reformulate the Xu-White model (see Appendix A) to apply it to tight sandstone and siltstone, where minerals are a mixture of quartz, potassium feldspar, plagioclase, carbonate fragments and clay. We consider soft pores (clay pores and microfractures) and stiff pores (mainly in feldspar) and an oil-water mixture.

Three steps are considered, where we obtain the stiffness moduli of (1) the mineral mixture; (2) the dry rock; and (3) the wet rock. See the workflow in Fig. 6.

### Critical-porosity model

In the course of diagenesis, porosity gradually decreases to zero with compaction and cementation. As shown in Fig. 7, a critical porosity exist during this process, when the porosity is less than a critical value, the constituent minerals aggregate together to form a load-bearing skeleton. When the porosity exceeds the critical porosity, the minerals are not load-bearing and the stress is transmitted mainly through the fluid (Nur, 1992).

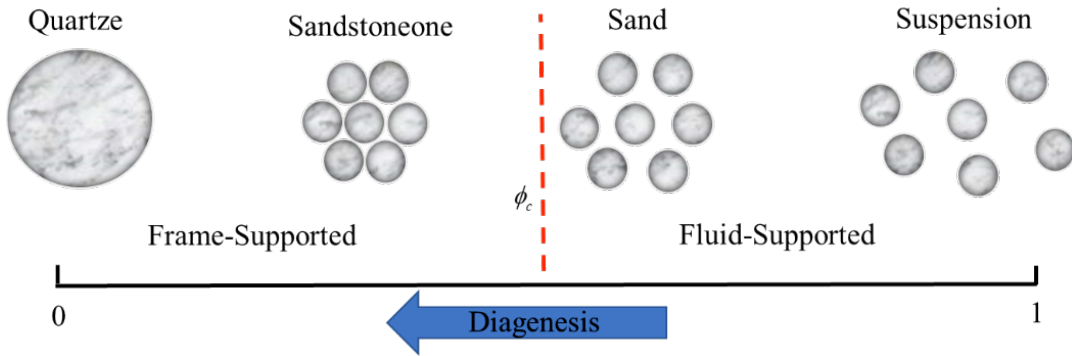


Fig. 7. Schematic diagram of critical porosity during rock consolidation (according to Nur et al., 1992).

Nur et al. (1992) propose

$$\left\{ \begin{array}{l} K_d = K_m \left(1 - \frac{\phi}{\phi_c}\right) \\ \mu_d = \mu_m \left(1 - \frac{\phi}{\phi_c}\right) \end{array} \right. , \quad (1)$$

where  $K_d$  and  $\mu_d$  are the dry-rock bulk and shear moduli,  $K_m$  and  $\mu_m$  are the mineral bulk and shear moduli,  $\phi$  and  $\phi_c$  are the porosity and critical porosity, respectively. Nur et al. (1992) considered that the critical porosity depends on the rock type. For example,  $\phi_c \approx 0.6$  and  $\phi_c \approx 0.4$  for dolomite and sandstone, respectively. In tight sandstones and shales, the critical porosity is difficult to determine.

To obtain  $K_m$  and  $\mu_m$ , the Voigt-Reuss-Hill and Hashin-Shtrikman-Hill averages or time-average equation can be applied (e.g., Qadrouh et al., 2020). When the rock components and their combinations are relatively complex, the self-consistent theory can be used instead, while for rocks with a few components and tight structure, the Voigt-Reuss-Hill average is

$$\begin{cases} \rho_m = \sum_{i=1}^N f_i \rho_i \\ K_m = \sum_{i=1}^N f_i K_i + \sum_{i=1}^N \frac{f_i}{K_i} \\ \mu_m = \sum_{i=1}^N f_i \mu_i + \sum_{i=1}^N \frac{f_i}{\mu_i} \end{cases}, \quad (2)$$

where  $K_i$  and  $\mu_i$  are the bulk and shear moduli of the minerals, and  $\rho_i$  their density. The mineral/fluid properties are given in Table 1.

Table 1. Physical properties of the rock (Mavko et al., 1988).

Mineral/Fluid	Density (g •cm <sup>-3</sup> )	Bulk modulus (GPa)	Shear modulus (GPa)
Quartz	2.65	37	44
Potassium Feldspar	2.56	48	24
Plagioclase	2.63	75.6	25.6
Calcite	2.71	76.8	32
Clay	2.6	21	7
Water	1	2.25	0
Oil	0.8	1.02	0

### Bulk modulus of the fluid mixture

Three methods can be used to compute the bulk modulus of the fluid mixture: (1) Brie et al. (1995) for gas-fluid patchy mixtures; (2) The isostress Wood equation when the fluids are microscopically mixed; (3) Voigt equation as an upper limit in the patchy case.

We use the Wood equation:

$$K_f = \left( \frac{S_w}{K_w} + \frac{S_o}{K_o} \right)^{-1}, \quad (3)$$

where,  $K_w$ ,  $K_o$  and  $S_w$ ,  $S_o$  are the bulk moduli and saturations of water and oil, respectively, the latter satisfy  $S_w + S_o = 1$ .

The composite density is

$$\rho_f = S_w \rho_w + S_o \rho_o, \quad (4)$$

where  $\rho_w$  and  $\rho_o$  are the densities of water and oil, respectively.

### Determination of the critical porosity

Let us introduce a critical-porosity parameter  $D=1-\phi/\phi_c$ . In order to obtain  $D$ , the critical-porosity model and Maxwell-BISQ model are combined to compute the P-wave velocities, and an objective function is established by considering a known experimental P-wave velocity (e.g., from logs) and the theoretical velocity.

When the porefill is a Maxwell fluid, following Dvorkin et al. (1993), in order to take into account the squirt-flow mechanism in the Biot-Tsiklauri model, we replace the viscosity correction factor  $F(\omega)$  (Cui et al., 2004) in the BISQ model with  $F_M(\omega)$  (Cui et al. 2003, 2010).

$$F_M(\omega) = i(\omega/\omega_c)Z(\omega)/[Z(\omega)-1]. \quad (5)$$

where

$$Z(\omega) = \int_0^\infty 2J_1(\beta a)/[\beta a J_0(\beta a)]f(a)da,$$

$$\beta^2 = (\omega^2 t_M + i\omega)\rho_f/\eta,$$

where  $F_M(\omega)$  is the viscosity correction factor which is generalized to the case of a Maxwell fluid with an arbitrary pore size distribution (Cui et al., 2003),  $\omega$  and  $\omega_c$  are the angular and Biot's transition frequency, respectively,  $t_M$  is the relaxation time (hereafter M denotes Maxwell),  $J_0$  and  $J_1$  are Bessel functions of orders zero and one, and  $\eta$  is the fluid viscosity. The general equations that govern wave propagation in non-Newtonian (Maxwell) fluid-saturated porous media are given in Appendix B.

The P-wave velocities are

$$V_{p1,2}(D) = 1 / \operatorname{Re} \sqrt{Y_{p1,2}} \quad , \quad (6)$$

where P1 and P2 denote compressional waves of the first kind and second kind, respectively.

The roots  $Y$  are determined from

$$c_2 Y^2 - c_1 Y + c_0 = 0 \quad , \quad (7)$$

where

$$c_2 = \hat{H}\hat{M} - C^2,$$

$$c_1 = \hat{H}\rho_{\text{eff}} + \hat{M}\rho - 2\rho_f \hat{C},$$

$$c_0 = \rho\rho_{\text{eff}} - \rho_f^2,$$

$$\hat{H} = K_d + \frac{4\mu_d}{3} + (1 - K_d / K_m)^2 \hat{M},$$

$$\hat{C} = (1 - K_d / K_m) \hat{M},$$

$$\hat{M} = MS_M(\omega),$$

$$M = K_f K_m / [\phi K_m + (1 - K_d / K_m - \phi) K_f],$$

$$\rho_{\text{eff}} = i\eta / [\omega \kappa_M(\omega)],$$

$$\kappa_M(\omega) = \kappa_0 [F_M(\omega) - i\omega / \omega_c]^{-1} \quad ,$$

$$S_M(\omega) = 1 - 2J_1(\lambda_M R) / [\lambda_M R J_0(\lambda_M R)] \quad ,$$

$$\lambda_M = \omega \sqrt{\rho_{\text{eff}}(\omega) / M} \quad ,$$

where  $\omega$  and  $\omega_c$  are the angular and Biot frequencies, respectively,  $\kappa_0$  and  $\kappa_M(\omega)$  are the static and dynamic permeabilities, respectively,  $\eta$  is the fluid viscosity,  $R$  is the characteristic squirt-flow length,  $\rho_{\text{eff}}$  is the effective density of the fluid in relative motion, and  $\rho$  is the composite density, i.e.,  $\rho = \rho_m(1 - \phi) + \rho_f \phi$ .

The objective function minimizes the difference between the model and experimental velocities,

$$\varepsilon = |V_p(D) - V_p| \quad , \quad (8)$$

where  $V_p(D)$  is the P-wave velocity from eq. (6), and  $V_p$  is the experimental one.

An iterative algorithm is used to solve the objective function to obtain the optimal  $D$

### S velocity based on $D$

By substituting  $D$  into eq. (1), we obtain the dry-rock shear modulus  $\mu_d$  and the S-wave velocity as

$$\mu_{\text{sat}} = \mu_d \quad , \quad (9)$$

$$V_s = \sqrt{\frac{\mu_{\text{sat}}}{\rho}} \quad . \quad (10)$$

where  $\mu_{\text{sat}}$  is the fluid-saturated rock shear moduli.

## EXAMPLES

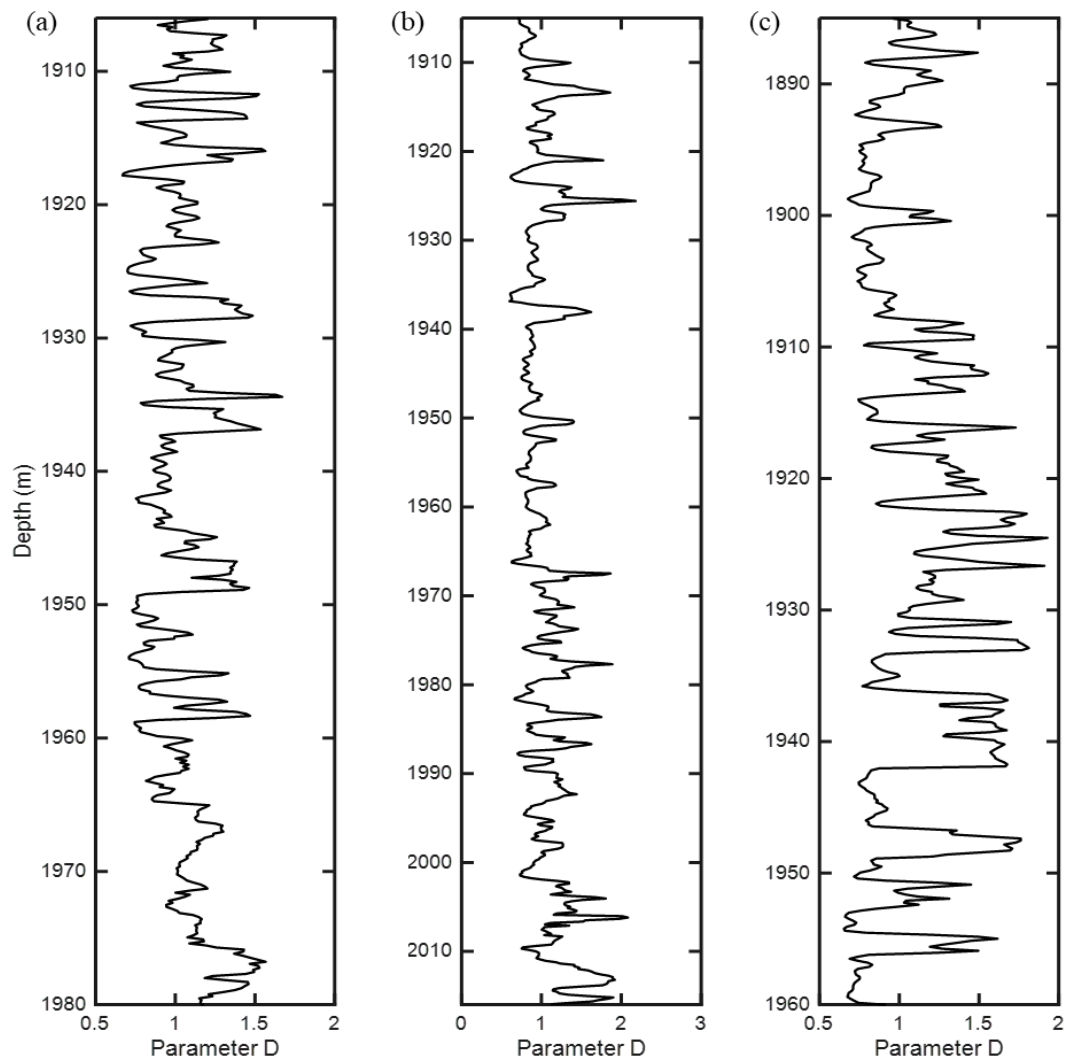
To validate the method, log data from the Qingyang area, Ordos Basin, are considered, which is mainly located within the  $7_1$ - $7_2$  sections of the Chang 7 Member. The target layers are mainly tight sandstones and siltstones, and the lithology distribution is complex. It is difficult to identify the lithology according to wave impedance. We have S log data in three wells, which are used for calibration.

Wells A, B and C with S-wave velocity logs are considered in the examples. The depth of the target layer in well A is 1906 ~ 1980 m, and the oil-bearing layers are in the ranges 1920 ~ 1923 m and 1949 ~ 1952 m. The same quantities for well B are 1905 ~ 2016 m, and 1930 ~ 1935 m, 1939 ~ 1948 m, 1952 ~ 1956 m and 1961 ~ 1964 m. For well C, we have 1885 ~ 1960 m, and 1894 ~ 1899 m, 1901 ~ 1905 m and 1957 ~ 1960 m, respectively.

The main input parameters are density, porosity, shale content, water saturation, and P-wave velocity. Fig. 8 shows  $D$  obtained with eq. (8) and the three well logs. Figs. 9 - 11 respectively give the logging curves of wells A, B and C, as well as the predicted S-wave velocity and relative error. The two sets show a good agreement. We compute the relative error between the classical Xu-White model and the reformulated model in Table 2. As can be seen, the latter model improves the prediction, where the average relative error of the three wells is 4.3-4.8%.

Table 2. Average relative errors of the S-wave prediction of the two models.

Well	Relative error of the reformulated model (%)	Relative error of the classical Xu-White model (%)
A	4.3	10.8
B	4.6	9.4
C	4.8	12

Fig. 8.  $D$  variation with depth in well A (a), well B (b) and well C (c).

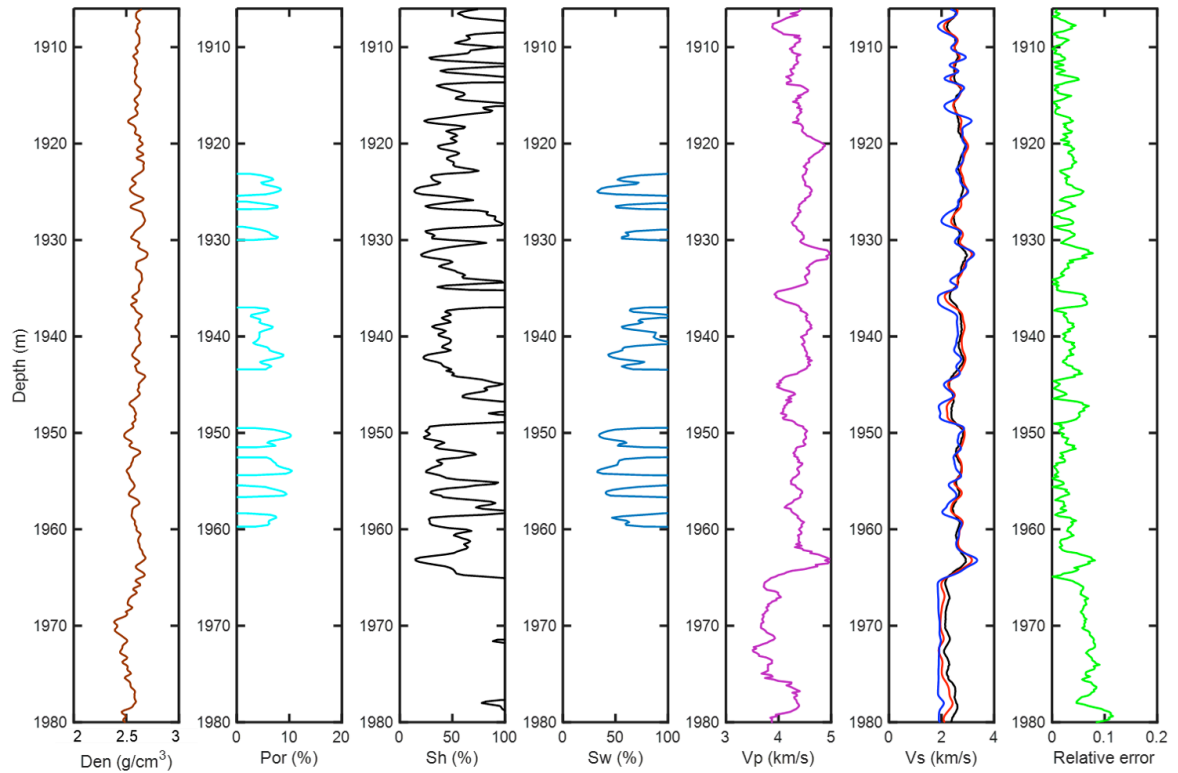


Fig. 9. Logs of density (Den), porosity (Por), shale content (Sh), water saturation (Sw), P-wave velocity ( $V_p$ ) and S-wave velocity ( $V_s$ ) in Well A. The red curve denotes the estimated S-wave velocity by the reformulated model, the blue curve denotes the S-wave velocity by the classical Xu-White model, and the relative error is given.

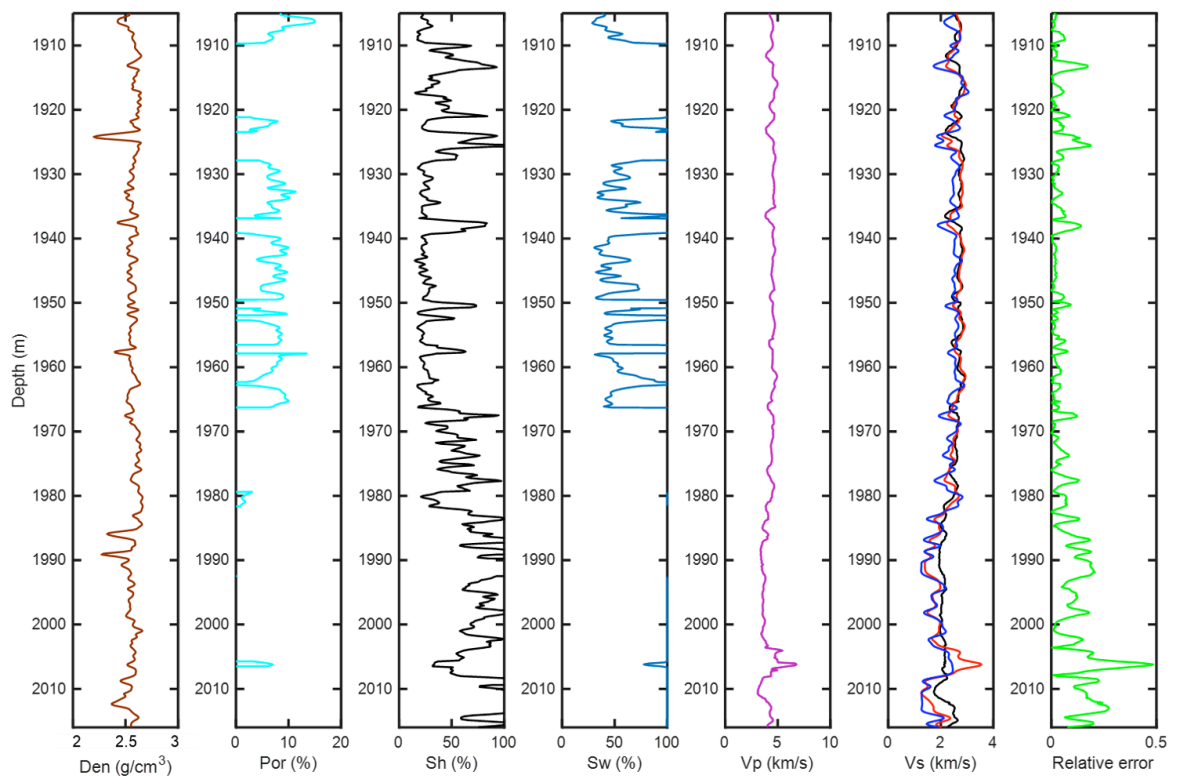


Fig. 10. Same as Fig. 9 for well B.

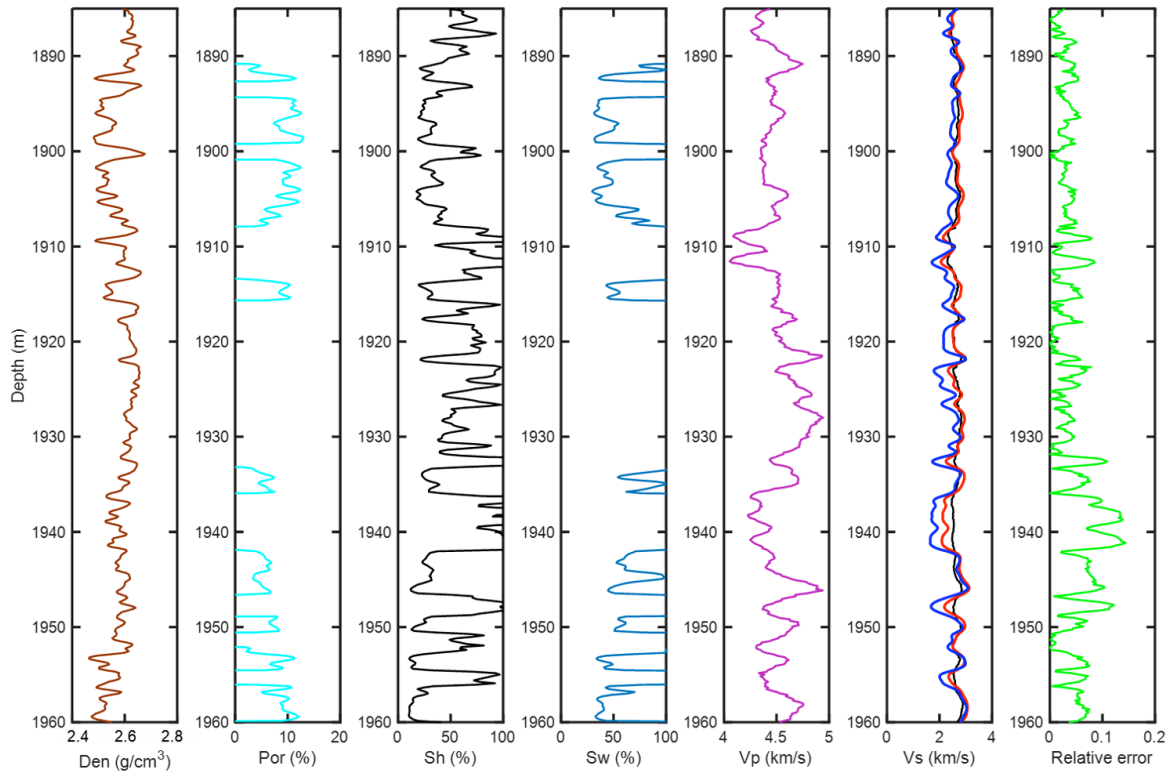


Fig. 11. Same as Fig. 9 for well C.

The distribution diagram of the S-wave velocity error corresponding to the two models is shown in Figs. 12-14, where we can see that the error of the classical Xu-White model is higher.

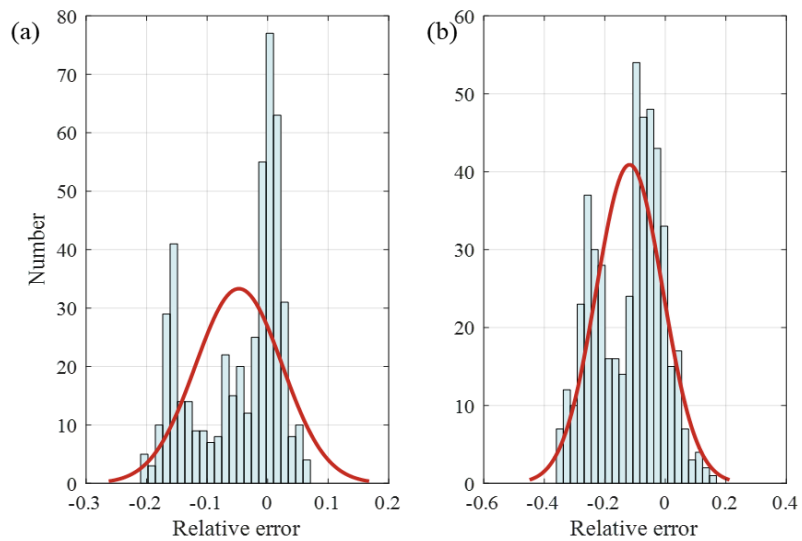


Fig. 12. Error in Well A corresponding to the reformulated model (a) and classical Xu-White model (b).

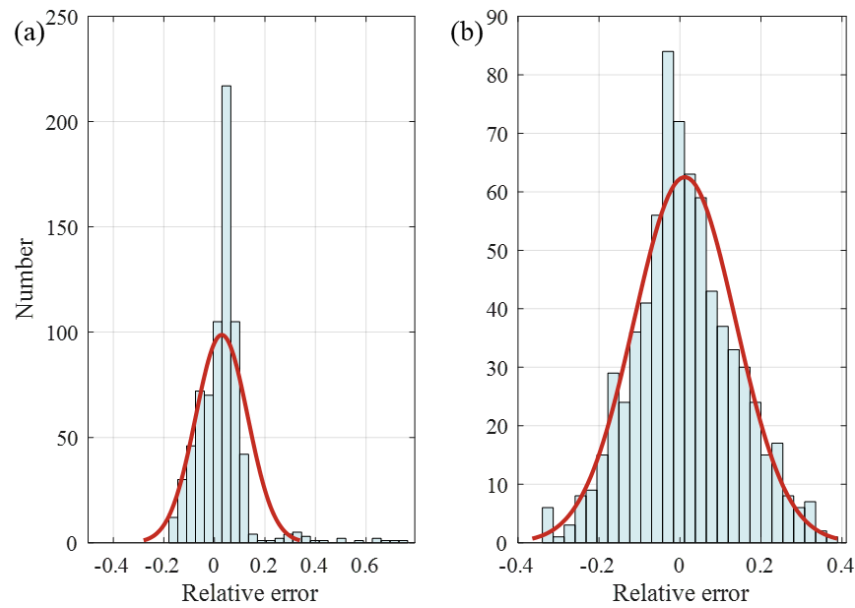


Fig. 13 Same as Fig. 12 for well B.

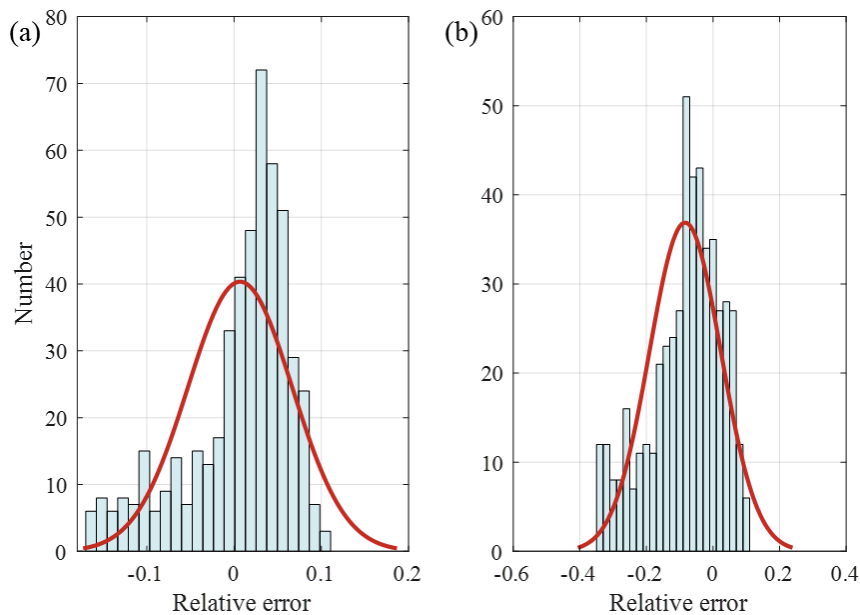


Fig. 14. Same as Fig. 12 for well C.

Figs. 15, 16 and 17 show crossplots between the estimated and experimental S-wave velocities in wells A, B and C, respectively. The estimated values of the reformulated model correlate better with the experimental ones. Fig. 16 (a) shows that there are larger errors within the zone indicated by the red rectangle. By checking the log data of Well B, these scatters are considered as anomalies. All Figs. (b) show that the classical model has large errors when the shale content is relatively high (see blue rectangles).

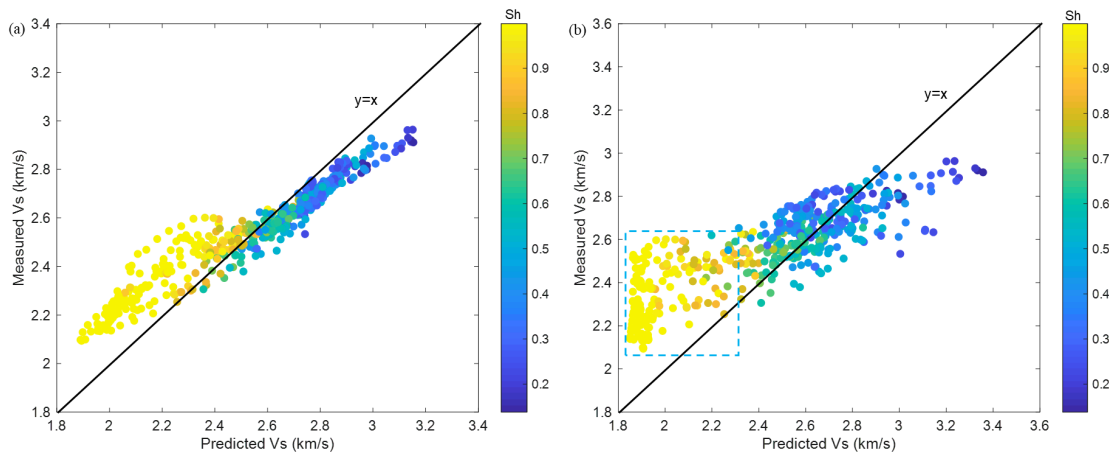


Fig. 15. Crossplot of the measured and estimated S-wave velocities in Well A by the reformulated (a) and classical Xu-White (b) models.

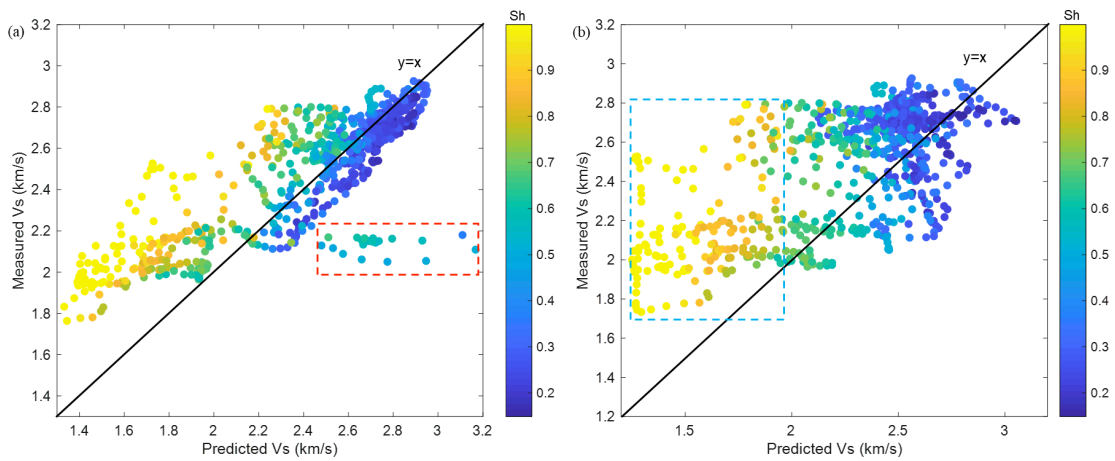


Fig. 16. Same as Fig. 15 for well B.

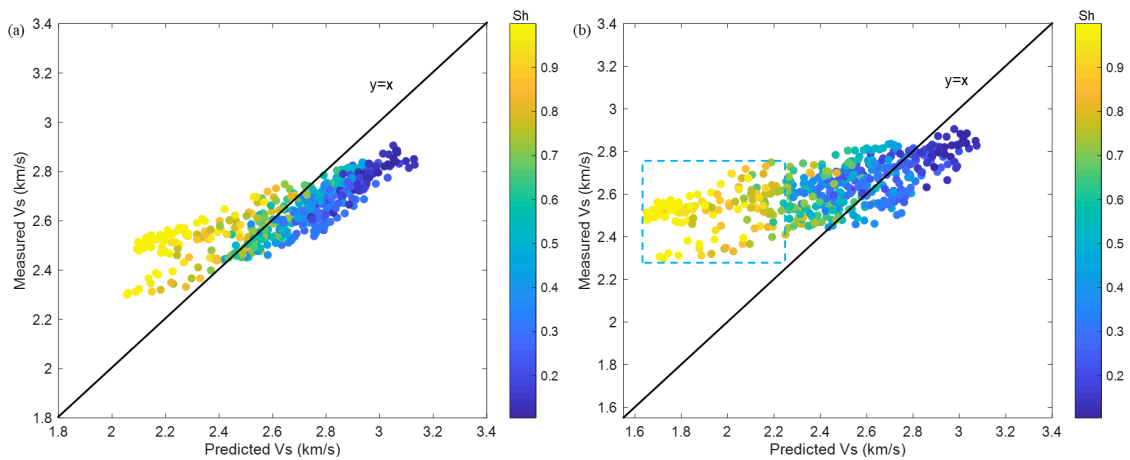


Fig. 17. Same as Fig. 15 for well C.

The ratio of P- and S-wave velocities ( $V_p/V_s$ ) (and Poisson ratio) is a frequently-used attribute for reservoir assessment, lithology identification and rock physics research (Carcione and Cavallini, 2002; Lee, 2003; Bhuiyan and Holt, 2012; Bhakta and Landrø, 2014; Aryanti et al., 2018), and can be used as a quality control factor in S-wave velocity estimation.  $V_p/V_s$  of oil-saturated or gas-saturated rocks is generally less than that of water-saturated rocks (Vanorio et al., 2006). In general, the bulk modulus of in-situ water is higher than that of oil/gas, so the P-wave velocity of a water-saturated rock is higher than that saturated by oil and gas.

Figs. 18-20 show gamma ray (GR) and Poisson's ratio (PR) from the experimental velocities, and  $V_p/V_s$  as a function of depth for the three. The trends of the different curves are basically consistent. In particular, the black dotted line indicates the oil-bearing sections of the target formation. It can be seen that the  $V_p/V_s$  is relatively low in these sections.

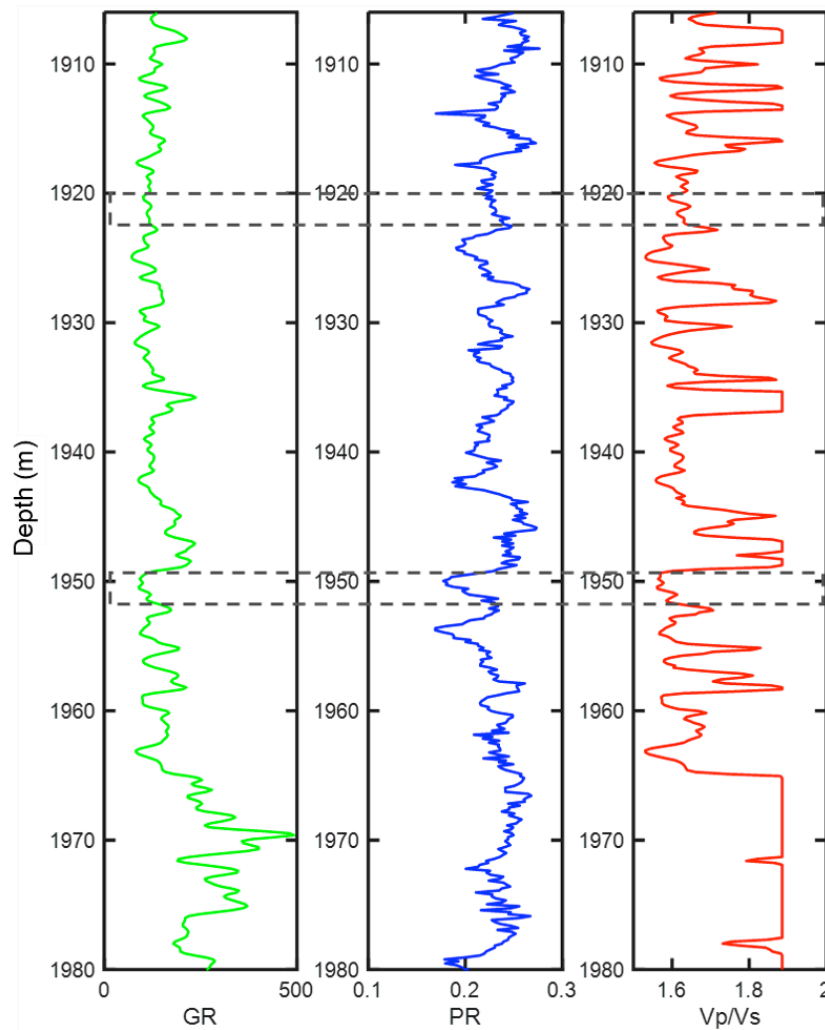


Fig. 18. Gamma ray, Poisson's ratio, and  $V_p/V_s$  as a function of depth in well A.

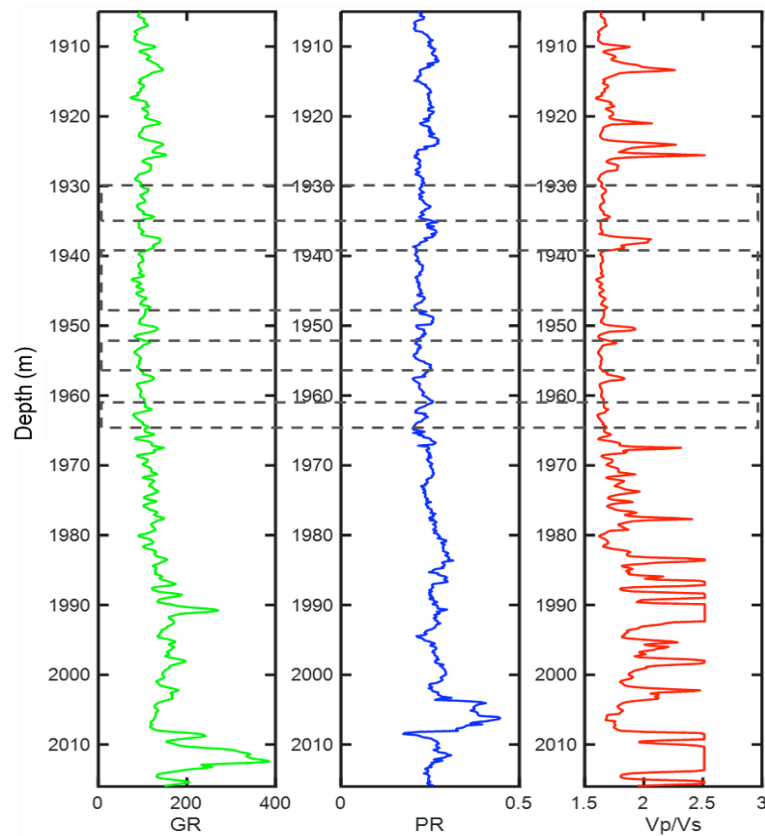


Fig. 19. Same as Fig. 18 for well B.

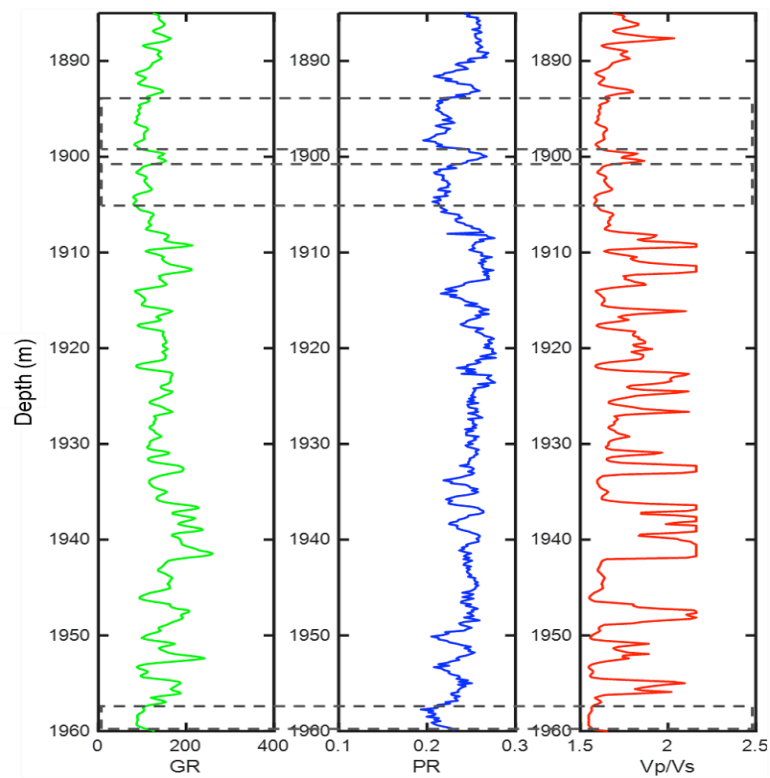


Fig. 20. Same as Fig. 18 for well C.

## CONCLUSIONS

We have developed a methodology based on the Xu-White model to estimate the S-wave velocity of shale-oil rocks, combining the critical-porosity and the Maxwell-BISQ models. An objective function considering the experimental (log) and theoretical wet-rock S-wave velocities is set to obtain the critical porosity as a function of depth, the dry-rock shear modulus and the wet-rock S-wave velocities to make predictions away from the well logs. Comparisons with the classical Xu-White model show that the velocities predicted by the reformulated model are in better agreement with the log data. The developed method can be useful to deal with complex pore-space configurations, such as those unconventional reservoirs.

## ACKNOWLEDGEMENTS

This work is supported by the National Natural Science Foundation of China (Grant No. 41974123, 42174161), the Jiangsu Innovation and Entrepreneurship Plan and the Jiangsu Province Science Fund for Distinguished Young Scholars (Grant No. BK20200021), the National Science and Technology Major Project of China (2017ZX05069-002).

## REFERENCES

- Aryanti, E., Nugraha, A.D., Basuki, A. and Triastuty, H., 2018. 3D seismic tomography Vp, Vs and Vp/Vs ratio beneath Gede Volcano, West Java, Indonesia. *Internat. Symp. Earth Hazard and Disaster Mitigation*.
- Ba, J., Xu, W.H., Fu, L.Y., Carcione, J.M. and Zhang, L., 2017. Rock anelasticity due to patchy-saturation and fabric heterogeneity: A double double-porosity model of wave propagation. *J. Geophys. Res. - Solid Earth*, 122: 1949-1976.
- Bhakta, T. and Landrø, M., 2014. Estimation of pressure-saturation changes for unconsolidated reservoir rocks with high Vp/Vs ratio. *Geophysics*, 79(5): M35-M54.
- Bhuiyan, M.H. and Holt, R.M., 2012. Vp-Vs ratio as a lithological indicator for shallow reservoir. *Extended Abstr., 74th EAGE Conf., Copenhagen*.
- Biot, M.A., 1956a. Theory of propagation of elastic waves in a fluid-saturated porous solid, I: Low-frequency range. *J. Acoust. Soc. Am.*, 28: 168-178.
- Biot, M.A., 1956b. Theory of propagation of elastic waves in a fluid-saturated porous solid, II: Higher-frequency range. *J. Acoust. Soc. Am.*, 28: 179-191.
- Biot, M.A., 1962. Mechanics of deformation and acoustic propagation in porous media, *J. Appl. Phys.*, 33: 1482-1498.
- Brown, R. and Korringa, J., 1975. On the dependence of the elastic properties of a porous rock on the compressibility of the pore fluid. *Geophysics*, 40: 608-616.
- Brie, A., Pampuri, F., Marsala, A.F. and Meazza, O., 1995. Shear sonic interpretation in gas-bearing sands. *SPE Ann. Techn. Conf. Exhibit., Dallas*.
- Carcione, J.M., 2014. *Wave Fields in Real Media, Theory and Numerical Simulation of Wave Propagation in Anisotropic, Anelastic, Porous and Electromagnetic Media (3rd ed.)*. Elsevier Science Publishers, Amsterdam.
- Carcione, J.M., and Cavallini, F., 2002. Poisson's ratio at high pore pressure. *Geophys. Prosp.*, 50: 97-106.
- Carcione, J.M., Gurevich, B. and Cavallini, F., 2000. A generalized Biot-Gassmann model for the acoustic properties of shaley sandstones. *Geophys. Prosp.*, 48: 539-557.

- Castagna, J.P., Batzle, M.L. and Eastwood, R.L., 1985. Relationships between compressional-wave and shear-wave velocities in clastic silicate rocks. *Geophysics*, 50: 571-581.
- Cui, Z.W., Liu, J.X. and Wang, K.X., 2003. Elastic waves in non-Newtonian (Maxwell) fluid-saturated porous media. *Waves Rand. Med.*, 13: 191-203.
- Cui, Z.W., Wang, K.X., Cao, Z.L. and Hu, H.S., 2004. Slow waves propagation in BISQ poroelastic mode. *Chin. J. Geophys.*, 53: 3083-3089.
- Cui, Z.W., Liu, J.X., Wang, C.X. and Wang, K.X., 2010. Elastic waves in Maxwell fluid-saturated porous media with the squirt flow mechanism. *Chin. J. Geophys.*, 59: 8655-8661.
- Dvorkin, J. and Nur, A., 1993. Dynamic poroelasticity: A unified model with the Squirt and the Biot mechanisms. *Geophysics*, 58: 524-533.
- Dvorkin, J., Hoeksema, R.N. and Nur, A., 1994. The squirt-flow mechanism: macroscopic description. *Geophysics*, 59: 428-438.
- Downton, J.E., 2005. Seismic Parameter Estimation from AVO Inversion. University of Calgary, Department of Geology and Geophysics.
- EIA, 2013. Technically Recoverable Shale Oil and Shale Gas Resources: An Assessment of 137 Shale Formations in 41 Countries Outside the United States. Washington DC: U.S. Department of Energy.
- Gassmann, F., 1951. Über die Elastic Poroser Media. *Vierteljahrschrift der Naturforschenden Gesellschaft in Zürich*, 96: 1-23.
- Gholami, R., Moradzadeh, A., Rasouli, V. and Hanachi, J., 2014. Shear wave velocity prediction using seismic attributes and well log data. *Acta Geophys.*, 62: 818-848.
- Han, D., Nur, A. and Morgan, D., 1986. Effect of porosity and Clay content on wave velocity in sandstones. *Geophysics*, 51: 2093-2107.
- Krief, M., Garat, J., Stellingwerf, F.J. and Ventre, J., 1990. A petrophysical interpretation using the velocities of P- and S-waves (full-waveform sonic). *Log Analyst*, 31: 355-369.
- Kuster, G.T. and Toksöz, M.N., 1974. Velocity and attenuation of seismic waves in two-phase media: Part I. Theoretical formulations. *Geophysics*, 39: 587.
- Lee, M.W., 2003. Velocity Ratio and its Application to Predicting Velocities: US Department of the Interior, US Geological Survey.
- Li, L., Ma, J.F., Wang, H.F., Tan, M.Y., Cui, S.L., Zhang, Y.Y. and Qu, Z.P., 2017. Shear wave velocity prediction during CO<sub>2</sub>-EOR and sequestration in the gao89 well block of the Shengli oilfield. *Appl. Geophys.*, 14: 372-380.
- Li, Q., 1992. Velocity regularities of P- and S-waves in formations. *Oil Geophys. Prosp.*, 27: 1-12.
- Mavko, G.M. and Nur, A., 1975. Melt squirt in the asthenosphere. *J. Geophys. Res.*, 80: 1444-1448.
- Mavko, G., Mukerji, T. and Dvorkin, J., 1988. *The Rock Physics Handbook: Tools for Seismic Analysis in Porous Media*. Cambridge University Press, Cambridge.
- Nur, A. and Simmons, G., 1969. The effect of saturation on velocity in low porosity rocks. *Earth Planet. Sci. Lett.*, 7: 183-193.
- Nur, A., 1992. Critical porosity and the seismic velocities in rocks. *EOS Transact. AGU*, 73: 43-66.
- Parvizi, S., Kharrat, R., Asef, M.R., Jahangiry, B. and Hashemi, A., 2015. Prediction of the shear wave velocity from compressional wave velocity for the Gachsaran formation. *Acta Geophys.*, 63: 1231-1243.
- Pickett, G.R., 1963. Acoustic character logs and their applications in formation evaluation. *J. Petrol. Technol.*, 15: 650-667.
- Pang, M.Q., Ba, J., Carcione, J.M., Picotti, S., Zhou, J. and Jiang, R., 2019. Estimation of porosity and fluid saturation in carbonates from rock-physics templates based on seismic Q. *Geophysics*, 84(6): M25-M36.
- Qadrouh, A.N., Carcione, J.M., Alajmi, M. and Alyousif, M.M., 2019. A tutorial on machine learning with geophysical applications. *Boll. Geofis. Teor. Applic.*, 60: 375-402.
- Qadrouh, A.N., Carcione, J.M., Alajmi, M. and Ba, J., 2020. Bounds and averages of seismic quality factor Q. *Studia Geophys. Geodaet.*, 64: 100-113.

- Smith, G.C. and Gidlow, M., 2000. A comparison of the fluid factor with  $\lambda$  and  $\mu$  in AVO analysis. Expanded Abstr., 70th Ann. Internat. SEG Mtg., Calgary: 2484.
- Tsiklauri, D., 2002. Phenomenological model of propagation of the elastic waves in a fluid-saturated porous solid with non-zero boundary slip velocity. *J. Acoust. Soc. Am.*, 112: 843-849.
- Tan, M.J., Peng, X., Cao, H.L., Wang, S.X. and Yuan, Y.J., 2015. Estimation of shear wave velocity from wireline logs in gas-bearing shale. *J. Petrol. Sci. Engineer.*, 133: 352-366.
- Vanorio, T. and Mavko, G., 2006. Vp/Vs ratio in gas-pressured saturated sandstones. Expanded Abstr., 76th Ann. Internat. SEG Mtg., New Orleans: 3541.
- Vernik, L., Castagna, J. and Omovie, S.J., 2017. Shear-wave velocity prediction in unconventional shale reservoirs. *Geophysics*, 83(1): 1-43.
- White, J.E., 1965. *Seismic Waves: Radiation, Transmission, and Attenuation*. McGraw-Hill Book Co., New York.
- Xu, S. and White, R.E., 1995. A new velocity model for clay-sand mixtures. *Geophys. Prosp.*, 43: 91-118.
- Xu, S. and White, R.E., 1996. A physical model for shear wave velocity prediction. *Geophys. Prosp.*, 44: 687-717.
- Yan, J., Lubbe, R. and Pillar, N., 2007. Variable aspect ratio method in the Xu-White model for AVO. Extended Abstr., 69th EAGE Conf., London.
- Zhang, J.F., Bi, H.B., Xu, H., Zhao, J.L., Zhao, D. and Geng, J.G., 2015. New progress and reference significance of overseas tight oil exploration and development. *Acta Petrol. Sinica*, 36: 127-137.
- Zhang, L., Ba, J., Carcione, J.M. and Sun, W.T., 2019. Modeling wave propagation in cracked porous media with penny-shaped inclusions. *Geophysics*, 84(4): WA141-WA151.
- Zhang, L., Ba, J. and Carcione, J.M., 2021. Wave propagation in infinituple-porosity media. *J. Geophys. Res. - Solid Earth*, 126: e2020JB021266.
- Zhou, L.H., Pu, X.G., Xiao, D.Q., Li, H.X. and Qu, N., 2018. Geological conditions for shale oil formation and the main controlling factors for the enrichment of the 2nd member of Kongdian Formation in the Cang dong Sag, Bohai Bay Basin. *Nat. Gas Geosci.*, 29: 1323-1332.
- Zou, C.N., Tao, S.Z., Yang, Z., Hou, L.H., Yuan, X.J., Zhu, R.K., Jia, J.H., Wu, S.T., Gong, Y.J., Gao, X.H., Wang, L. and Wang, J., 2013. Development of petroleum geology in china: discussion on continuous petroleum accumulation. *J. Earth Sci.*, 24: 796-803.

## APPENDIX A

### XU-WHITE MODEL

The Xu-White model considers an argillaceous sandstone with small and large aspect-ratio pores, present the shaley and sandy parts, respectively. The bulk and shear moduli of the dry rock are calculated by using Kuster-Toksöz model (1974) and differential equivalent medium theory (DEM). The equations are

$$\phi = \phi_{cl} + \phi_s, \quad (A-1)$$

$$\phi_{cl} = v_{cl} \frac{\phi}{1 - \phi}, \quad (A-2)$$

$$\phi_s = v_s \frac{\phi}{1-\phi}, \quad (\text{A-3})$$

$$K_d - K_m = \frac{1}{3}(K_f - K_m) \frac{3K_d + 4\mu_m}{3K_m + 4\mu_m} \sum_{l=c,s} \phi_l T_{ijj}(\alpha_l), \quad (\text{A-4})$$

$$\mu_d - \mu_m = \frac{\mu_f - \mu_m}{5} \frac{6\mu_d(K_m + 2\mu_m) + \mu_m(9K_m + 8\mu_m)}{5\mu_m(3K_m + 4\mu_m)} \sum_{l=c,s} \phi_l F(\alpha_l), \quad (\text{A-5})$$

$$F(\alpha) = T_{ijj}(\alpha_l) - \frac{T_{ijj}(\alpha_l)}{3}, \quad (\text{A-6})$$

where  $\phi_{cl}$  and  $\phi_s$  are the shaly and sandy porosities, respectively,  $v_{cl}$  and  $v_s$  are their corresponding volume percentages,  $\alpha_l$  is the aspect ratio. The scalars  $T_{ijj}$  and  $T_{ijj}$  are functions of the aspect ratio, and the properties of the matrix and the fluid are given in Appendix C.

The Gassmann equation (Gassmann, 1951; Carcione, 2014) model is used to obtain the P-wave velocity:

$$K_{\text{sat}} = K_d + \frac{\left(1 - \frac{K_d}{K_m}\right)^2}{\frac{\phi}{K_f} + \frac{1-\phi}{K_m} - \frac{K_d}{K_m^2}}, \quad (\text{A-7})$$

where  $K_{\text{sat}}$  is the fluid-saturated rock bulk moduli.

The fluid-saturated rock P- and S-wave velocities are calculated by

$$V_p = \sqrt{\frac{K_{\text{sat}} + \frac{4}{3}\mu_{\text{sat}}}{\rho}}, \quad (\text{A-8})$$

$$V_s = \sqrt{\frac{\mu_{\text{sat}}}{\rho}}. \quad (\text{A-9})$$

## APPENDIX B

The general equations that govern wave propagation in non-Newtonian (Maxwell) fluid-saturated porous media are (Cui et al., 2010)

$$\begin{aligned} \mu_d \nabla^2 u + (\hat{H} - \mu_d) \nabla \nabla \cdot u + \hat{C} \nabla \cdot w &= \rho \ddot{u} + \rho_f \dot{w} \\ \nabla (\hat{C} \nabla \cdot u + \hat{M} \nabla \cdot w) &= \rho_f \ddot{u} + \rho_{\text{eff}} \dot{w} \end{aligned} \quad (\text{B-1})$$

where  $u$  and  $w$  are the skeleton and fluid displacement vectors, respectively.

## APPENDIX C

### COEFFICIENTS OF THE KUSTER AND TOKSÖZ THEORY

$$T_{ijj} = \frac{3F_1}{F_2}, \quad (\text{C-1})$$

$$T_{ijj} - \frac{1}{3} T_{ijj} = \frac{2}{F_3} + \frac{1}{F_4} + \frac{F_4 F_5 + F_6 F_7 - F_8 F_9}{F_2 F_4}, \quad (\text{C-2})$$

where

$$F_1 = 1 + A \left[ \frac{3}{2} (g + \vartheta) - P \left( \frac{3}{2} g + \frac{5}{2} \vartheta - \frac{4}{3} \right) \right],$$

$$\begin{aligned} F_2 = 1 + A \left[ 1 + \frac{3}{2} (g + \vartheta) - \frac{P}{2} (3g + 5\vartheta) \right] + B(3 - 4P) \\ + \frac{A}{2} (A + 3B)(3 - 4P) [g + \vartheta - P(g - \vartheta + 2\vartheta^2)], \end{aligned}$$

$$F_3 = 1 + \frac{A}{2} \left[ P(2 - \vartheta) + \frac{1 + \alpha^2}{\alpha^2} g(P - 1) \right],$$

$$F_4 = 1 + \frac{A}{4} [3\vartheta + g - P(g - \vartheta)],$$

$$F_5 = A \left[ P \left( g + \vartheta - \frac{4}{3} \right) - g \right] + B\vartheta(3 - 4P),$$

$$F_6 = 1 + A[1 + g - P(g + \vartheta)] + B(1 - \vartheta)(3 - 4P),$$

$$F_7 = 2 + \frac{A}{4} [9\vartheta + 3g - P(5\vartheta + 3g)] + B\vartheta(3 - 4P),$$

$$F_8 = A \left[ 1 - 2P + \frac{g}{2} (P - 1) + \frac{\vartheta}{2} (5P - 3) \right] + B(1 - \vartheta)(3 - 4P),$$

$$F_0 = A[g(P-1) - P\vartheta] + B\vartheta(3-4P),$$

$$A = \frac{\mu'}{\mu} - 1,$$

$$B = \frac{1}{3} \left( \frac{K'}{K} - \frac{\mu'}{\mu} \right),$$

$$P = \frac{3\mu}{3K + 4\mu},$$

$$g = \frac{\alpha^2}{1-\alpha^2} (3\vartheta - 2),$$

$$\vartheta = \frac{\alpha}{(1-\alpha^2)^{3/2}} [\cos^{-1} \alpha - \alpha(1-\alpha^{1/2})],$$

where  $K$  and  $\mu$  are the bulk and shear moduli of the solid in which the pores are embedded, and  $K'$  and  $\mu'$  those of the inclusions.